A conserved protonation-dependent switch controls drug binding in the Abl kinase

Yibing Shan[a], Markus A. Seeliger[b], Michael P. Eastwood[a], Filipp Frank[b], Huafeng Xu[a], Morten Ø. Jensen[a], Ron O. Dror[a], John Kuriyan[b,1], and David E. Shaw[a,c,1]

[a]D. E. Shaw Research, New York, NY 10036; [b]Howard Hughes Medical Institute, Department of Molecular and Cell Biology and Department of Chemistry, University of California, Berkeley, CA 94720; and [c]Center for Computational Biology and Bioinformatics, Columbia University, New York, NY 10032

Contributed by John Kuriyan, November 13, 2008 (sent for review September 29, 2008)

In many protein kinases, a characteristic conformational change (the "DFG flip") connects catalytically active and inactive conformations. Many kinase inhibitors—including the cancer drug imatinib—selectively target a specific DFG conformation, but the function and mechanism of the flip remain unclear. Using long molecular dynamics simulations of the Abl kinase, we visualized the DFG flip in atomic-level detail and formulated an energetic model predicting that protonation of the DFG aspartate controls the flip. Consistent with our model's predictions, we demonstrated experimentally that the kinetics of imatinib binding to Abl kinase have a pH dependence that disappears when the DFG aspartate is mutated. Our model suggests a possible explanation for the high degree of conservation of the DFG motif: that the flip, modulated by electrostatic changes inherent to the catalytic cycle, allows the kinase to access flexible conformations facilitating nucleotide binding and release.

conformational change | DFG motif | imatinib | molecular dynamics simulation | pH dependence

Nearly 2% of human genes encode protein kinases (1), enzymes involved in almost all aspects of cellular regulation, which use ATP to phosphorylate protein substrates and release ADP as a byproduct. Given the importance of protein kinases to cell growth, movement, and death, it is not surprising that the protein kinase catalytic domain is the protein domain most commonly encoded by known cancer genes (2), and that protein kinases constitute one of the largest families of drug targets (3).

Lying within nearly every eukaryotic protein kinase domain, adjacent to the ATP-binding site, is a sequence of 3 residues, Asp-Phe-Gly (DFG). The reasons for the conservation of these residues are not fully understood, but the motif is known to be highly important, as was recently highlighted by the identification of potential "driver" mutations in human cancers at the DFG motif in 8 different kinases (4). The DFG aspartate is believed to be important for catalysis, and indeed typically points into the ATP-binding site (the DFG-in conformation), where it can coordinate an ATP-bound magnesium ion (5, 6). In a diverse subset of protein kinases, however, including c-Abl, IRK, c-Kit, Flt3, Csk, RAF, and P38, the DFG motif can also adopt a dramatically different conformation in which the DFG aspartate and phenylalanine side chains swap positions, leaving the aspartate pointing away from the binding site (the DFG-out conformation). The conformational change connecting the DFG-in and DFG-out conformations (a "DFG flip"; see Fig. 1) involves a ≈10-Å change in the positions of the 2 side chains.

The DFG flip (see Movie S1) is a central feature of the activation of the nonreceptor tyrosine kinase c-Abl, which before activation is held in an inactive DFG-out conformation by an autoinhibitory interaction with its regulatory domains (7). The DFG flip underlies the success of the cancer drug imatinib, which binds to the DFG-out conformation of the aberrant gene fusion product BCR-Abl (8) and has proven remarkably efficacious in the clinical treatment of chronic myeloid leukemia and certain other cancers (9, 10). The ability of imatinib to specifically recognize the DFG-out conformation of BCR-Abl has been credited for imatinib's selectivity, and intensive searches are now under way for other kinase inhibitors that selectively bind to DFG-out conformations (11, 12).

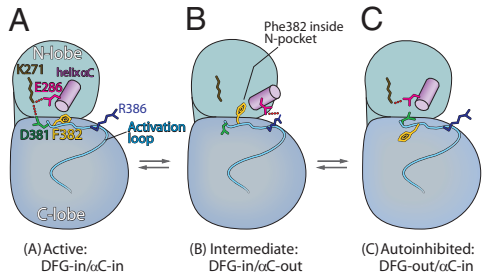

Fig. 1. A proposed mechanism for the DFG flip based on crystal structures and our Abl simulations. Key structural features are highlighted, with salt bridges represented by red dotted lines. The ATP-binding site is located between the N-lobe and the C-lobe. The active structure (*A*) and the autoinhibited structure (*C*) differ in their DFG conformation, and interconvert via a DFG flip. Nevertheless, these structures both adopt conformations referred to as αC-in, in which helix αC is close to the ATP-binding site so that the Lys-271–Glu-286 salt bridge may form. (*B*) The structure shown is taken from the simulations, and is a proposed intermediate in the DFG flip. This structure differs from *A* and *C* in 2 significant ways. First, helix αC is positioned away from the ATP-binding site so that Glu-286 may form a salt bridge with Arg-386 (an αC-out conformation). Second, the outward displacement of helix αC creates a pocket at the base of the N-lobe, which we refer to as the N-pocket, and which in *B* is occupied by Phe-382. The PDB ID codes of the structures on which the figure is based are 2F4J (*A*) and 1OPK (*C*). (1OPK contains regulatory domains, but only the kinase domain is shown here.)

Knowledge of the detailed mechanism and driving forces of DFG conformational change would deepen our understanding of kinase activation and open new directions in drug discovery. However, it is very challenging to directly probe the dynamics of this motif experimentally (13). Molecular dynamics (MD) simulation provides an alternative means to study kinase dynamics (14–16), but the time scale accessible to such studies has typically been restricted to between 100 ps and 10 ns. Observation of the DFG flip at such short time scales has required the introduction of artificial biasing forces (17), which can generate nonphysical trajectories and obscure the forces that actually drive the flip. In the work reported here, we used recently developed algorithms for the high-speed, parallel execution of MD simulations (18–21) to perform unbiased MD simulations, each hundreds of nanoseconds in length, of a construct

Author contributions: Y.S., J.K., and D.E.S. designed research; Y.S., M.A.S., and F.F. performed research; Y.S., M.A.S., M.P.E., and H.X. analyzed data; and Y.S., M.A.S., M.P.E., M.Ø.J., R.O.D., J.K., and D.E.S. wrote the paper.

The authors declare no conflict of interest.

Freely available online through the PNAS open access option.

[1]To whom correspondence may be addressed. E-mail: David.Shaw@DEShawResearch.com or kuriyan@berkeley.edu.

This article contains supporting information online at www.pnas.org/cgi/content/full/0811223106/DCSupplemental.

of human c-Abl containing only the kinase domain. (Because the kinase domains of c-Abl and BCR-Abl are identical in sequence, we refer to this common domain below as simply "Abl.") Our analysis of these simulations allowed us to formulate a model of key dynamic, energetic, and structural factors involved in DFG flips. To validate our model experimentally, we used fluorescence assays of Abl–imatinib binding to probe DFG conformation, the results of which confirmed our central computational findings.

Like other eukaryotic protein kinase domains, Abl consists of a smaller N-terminal lobe and a larger C-terminal lobe (the N-lobe and the C-lobe, respectively), with the ATP-binding site located between them. The N-lobe is composed of 5 β-strands and a helix referred to as αC, whereas the C-lobe is predominantly helical. The DFG motif borders the ATP-binding site and is located between the 2 lobes, at the N terminus of a flexible segment known as the activation loop. Fig. 1*A* and *C* shows Abl adopting DFG-in (22) and DFG-out (7) conformations, respectively, whereas Fig. 1*B* shows an important intermediate conformation observed in our simulations of the DFG flip. This conformation differs from the other 2 in that helix αC is displaced away from the binding site (the αC-out conformation, by contrast with the αC-in conformation shown in Fig. 1 *A* and *C*). A recently solved crystal structure of Abl also adopts an αC-out conformation, which has been suggested as a potential intermediate in the DFG flip (17). Although kinases in their active states adopt αC-in conformations, many kinases in their inactive states are known to adopt αC-out conformations, first defined in Cdk (23) and Src (24, 25) kinases, but now seen in many others—including EGFR (26), whose αC-out conformation is recognized by the cancer drug lapatinib. Thus, just as many kinases can access alternative conformations through a DFG flip, many kinases can access alternative conformations through a transition between αC-in and αC-out conformations.

To study the conformational changes associated with the DFG flip without introducing any biasing forces in our MD simulations, we "loosened" helix αC by mutating to alanine a methionine residue that previous studies suggested might be involved in stabilizing hydrophobic interactions between helix αC and the remainder of the protein. In our simulations of the resulting protein, we were able to observe the DFG flip and its coupling with helix-αC motion at an atomic level of detail. Analysis of these simulations led us to propose an energetic model in which the protonation state of Asp-381, which is influenced by local electrostatic interactions, serves as the switch that controls the flip. On the basis of our simulation results, we made certain predictions regarding the pH dependence of Abl–imatinib binding, then performed fluorescence quenching experiments to test these predictions. The results of these experiments were consistent with our model (and also allowed us to estimate the time scale of the DFG flip to be tens of milliseconds). Our findings could be interpreted as providing mechanistic support for the suggestion (27) that the DFG flip plays a significant role in the catalytic cycle of protein kinases by facilitating nucleotide binding and release.

Results and Discussion

Simulations of Abl. We performed a total of >2 μs of all-atom MD simulations of Abl in explicit water, using the OPLS-AA/L force field (28, 29) for proteins, with most individual simulations between 100 and 300 ns in length. All simulations were performed at constant temperature (300 K) and pressure (1 bar); see *SI Text*.

N-Pocket as Part of the DFG-Flip Pathway. Standard electrostatics calculations (30) (see *SI Text*) suggest that in a DFG-in structure of Abl [PDB ID code 2F4J; Young *et al.* (22)], the DFG aspartate has an elevated pK_a. In a DFG-out structure of Abl [PDB ID code 1OPK (7)] the DFG aspartate appears to be protonated and hydrogen bonded to a backbone carbonyl group. These observations led us to hypothesize that the protonation of the DFG aspartate might be an important determinant of DFG conformation, and we therefore performed simulations with the residue in different protonation states. We started 4 simulations in the active DFG-in conformation, including 2 (simulations 1a and 1b in Table S1) with Asp-381 protonated and 2 with Asp-381 deprotonated (simulations 2a and 2b). No DFG flip was observed in these simulations, suggesting that its time scale is much longer than the several hundred nanoseconds we simulated. This result is consistent with NMR studies of the p38 (13) and PKA (31) kinases, which are suggestive of microsecond- to millisecond-scale DFG motions.

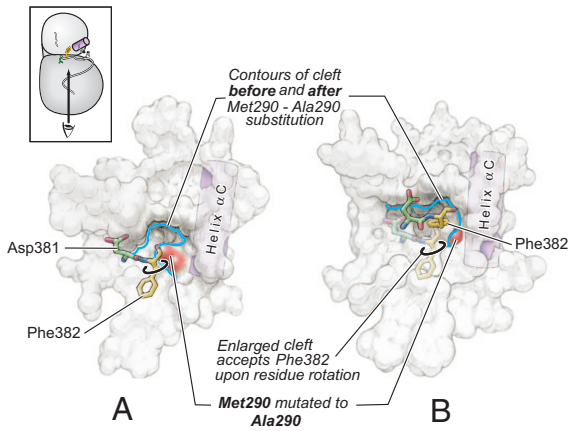

Fig. 2. The DFG motif and the N-pocket. Both *A* and *B* show the base of the N-lobe, with the C-lobe removed to make the N-pocket and DFG motif fully visible (see *Inset*). (*A*) An αC-out conformation illustrating the N-pocket. In this conformation the close interactions between Phe-382 and Met-290 have been transiently broken, but Met-290 still presents a steric barrier to the entry of Phe-382 into the N-pocket. This structure was taken from simulation 1a after 250 ns. (*B*) Phe-382 occupying the N-pocket, as enlarged by the M290A mutation. The motion through which Phe-382 enters the N-pocket (to yield a structure like that shown in Fig. 1*B*) principally involves a change of its χ_1 angle from approximately −60° to 60°. This structure is taken from simulation 4a after 2 ns. The conformation of Asp-381 and Phe-382 before Phe-382 enters the N-pocket is shown in a transparent rendering.

In all 4 simulations, however, substantial motion of helix αC was observed, despite the fact that no mutation was introduced to promote such motion. In the simulations with Asp-381 protonated, this motion was particularly pronounced, leading to the formation of the Glu-286–Arg-386 salt bridge characteristic of the αC-out conformation and emergence of a hydrophobic pocket (the N-pocket; see Fig. 1*B*) at the base of the N-lobe near Phe-382 (Fig. 2*A*). The N-pocket, which is contiguous with a region exploited by many drugs (the so-called "kinase specificity pocket"), has been suggested to play a role in facilitating the DFG flip (17). Although simulations 1a and 1b showed the transition from αC-in to αC-out (Fig. 1), we did not observe Phe-382 entering into the N-pocket, apparently because of interactions between this residue and the helix-αC residue Met-290. Likewise, we did not observe Phe-382 and Met-290 to adopt the exchanged positions they assume in crystal structures of Abl and Src kinases in αC-out conformations. These residues remained, for the most part, closely packed during the simulations (Fig. S1), and when they were briefly driven apart by thermal fluctuations, Met-290 remained a steric barrier at the entrance to the N-pocket (Fig. 2*A*).

To lower this barrier, we attempted to further increase the extent of motion of helix αC by introducing an M290A mutation. Met-290 is not a conserved residue in protein kinases, and the c-Src mutant corresponding to M290A maintains substantial activity (Fig. S2*B*). In Abl, Met-290 is part of a "hydrophobic spine" that stabilizes the active conformation (32), and we anticipated that the M290A mutation might therefore facilitate entry of Phe-382 into the N-pocket by allowing a larger range of motion of helix αC, as well as by directly reducing the size of the obstructing residue. We

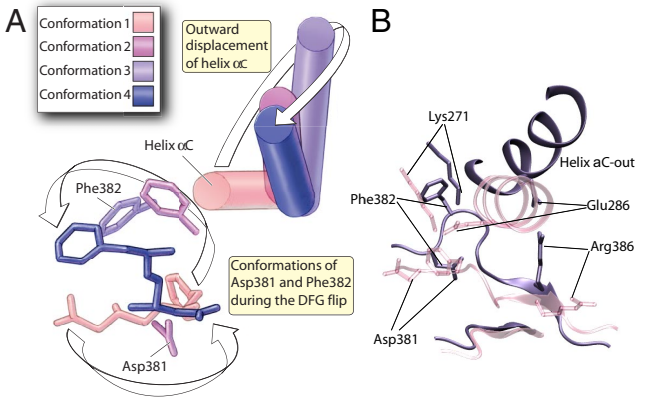

Fig. 3. Conformational change involved in the DFG flip. All simulation structures shown are taken from the same simulation of the DFG flip (6b). The active Abl crystal structure (PDB entry 2F4J) is shown in pink. (*A*) A DFG-in to DFG-out flip. As indicated by the arrows, starting from conformation 1 (the active structure), Asp-381 leaves the ATP-binding site by the C-lobe (lower) side, whereas Phe-382 enters from above via the N-pocket. Also shown is the displacement of helix αC accompanying the DFG flip. Conformations 2, 3 and 4 are taken from the simulation at 1, 75, and 122 ns, respectively. In the interest of clarity, Asp-381 in conformation 3 is not shown (Asp-381 adopts a very similar position in conformations 3 and 4). (*B*) Active Abl (pink) compared with a conformation taken from the simulation (purple) showing a typical displacement of helix αC and conformational change of the DFG main chain before the DFG flip. The significant difference between the 2 helix-αC conformations reflects in part the twist and hinge motion of the N-lobe relative to the C-lobe.

initiated simulations of the M290A mutant with the DFG aspartate both protonated (simulations 3 a–e) and deprotonated (4 a and b). With the M290A mutation, Phe-382 was indeed observed entering and leaving the N-pocket (Fig. 2*b*), with maximum residence times of 6 and 25 ns in simulations 4a and 4b, respectively. These results support the structural observation that Met-290 presents a barrier to the entry of Phe-382 into the N-pocket. Protonation of Asp-381 also appears to be a factor, because none of the simulations 3 a–e showed Phe-382 entering the N-pocket, presumably because of an indirect coupling between the (protonation-dependent) conformation of Asp-381 and the conformation of Phe-382. This failure of Phe-382 to enter the N-pocket when Asp-381 is protonated, however, may well be due to the limited simulation time scale, over which Asp-381 is trapped by a hydrogen bond (with Asp-363).

Simulations of the DFG-in to DFG-out Flip. Because the DFG-in conformation with Phe-382 in the N-pocket (Fig. 1*b*) may be an important intermediate of the DFG flip (17), we initiated 4 simulations of the M290A mutant from this conformation (taken from simulation 4a). In 2 simulations (5 a and b) Asp-381 was deprotonated and the DFG flip was not observed. In the other 2 simulations (6 a and b), Asp-381 was protonated and the DFG flip was observed after 68 and 76 ns, respectively. In our simulations, the M290A mutation was found to be required for Phe-382 to enter the N-pocket, but once this conformation had been reached, the DFG flip occurred even in the absence of this mutation. This was shown in simulation 7, which started from the same conformation, with Asp-381 protonated and Ala-290 mutated back to methionine; the DFG flip was observed after 33 ns. The 3 observed DFG flips followed similar pathways, as described below.

Fig. 3*A* shows a sequence of simulation conformations to illustrate the DFG flip. The motion of the 2 side chains through the crowded environment resembles a crankshaft motion around the main chain, and the DFG main chain also undergoes conformational rearrangement as an integral part of the flip (Fig. 3*B*).

The simulations indicate that large-scale motions play a key role in enabling the bulky side chain of Phe-382 to enter the ATP-binding site. Before the flip, we observe significant twisting and hinge-opening motions of the N-lobe with respect to the C-lobe, along with further outward displacement of helix αC leading to an αC-out conformation (Fig. 3). This leads to conformations in which Phe-382 has access to the ATP-binding site. After completion of the DFG flip, the N-lobe relaxes toward the autoinhibited conformation, and the interlobe motion subsides (Fig. S3).

A more detailed picture of the local changes occurring during the simulated DFG flip emerges from the examination of certain key dihedral angles. Several angles are different in the active and autoinhibited conformations (Fig. S4*B*). Protonation of Asp-381 at the beginning of the simulation causes this residue to reposition toward the C-lobe within the ATP-binding site, which is reflected in a change of its ϕ angle. There is subsequently significant motion, including large fluctuations in the ϕ angle of Gly-383 and concerted changes in most DFG main-chain dihedral angles (see Fig. S3). Until the DFG flip occurs, however, Asp-381 remains in the ATP-binding site and Phe-382 remains in the N-pocket, despite the main chain sometimes adopting DFG-out-like conformations. When the DFG motif finally flips, it is through a similar concerted change in main-chain conformation coupled with Phe-382 swinging into the ATP-binding site by means of a simultaneous change in its χ_1 angle. The flip itself lasts ≈2 ns. Subsequently, the dihedral angles in the DFG motif exhibit much less variation. Such a transition between relatively flexible and rigid states is observed in all 3 simulations in which we saw DFG flips.

Structural details of the DFG flip emerging from our simulations are consistent with existing crystal structures. Analysis of a representative set of kinase crystal structures (33) (see *SI Text*) shows that they and the simulation structures occupy similar regions of DFG conformational space (Fig. S4*B*). In both crystal structures and simulations, Asp-381 is always positioned toward the C-lobe side and Phe-382 toward the N-lobe whenever the DFG motif adopts an intermediate conformation between DFG-in and DFG-out. When ordered appropriately, the X-ray structures can even provide an "animation" of a DFG flip resembling the trajectory of the simulated conformational change (Fig. S4*A*).

DFG Conformation Is Controlled by a Protonation-Dependent Energetic Switch. We now construct a model of the relative free energy of the DFG-in and DFG-out conformations of Abl that can be used to estimate the effects of pH changes on DFG conformation. Although MD simulation could, in principle, be used to approximate such free energies, the aggregate amount of simulation time required to obtain accurate computational estimates using currently available techniques and technologies made this approach infeasible for use in this context. Instead, our model approximately accounts for the factors contributing to each conformation's stability by using empirical hydrophobicity data and a pK_a calculation on a static structure.

The most important structural factor embodied in our model is the change in environment of residues Asp-381 and Phe-382 caused by a DFG flip. In the DFG-in conformation, Asp-381 is located among charged and polar residues in the aqueous environment of the ATP-binding site, and Phe-382 is located in a hydrophobic environment. Conversely, after the DFG flip, Phe-382 is in the polar environment of the ATP-binding site, and Asp-381 is in a mostly hydrophobic environment. Because there is a very high free-energy cost to bury a charge in a hydrophobic environment (34), we assume DFG-out conformations to have Asp-381 protonated. Because our simulations point to the importance of the protonation state of this residue, our model contains 3 states: (*i*) DFG-in, Asp-381 deprotonated; (*ii*) DFG-in, Asp-381 protonated; and (*iii*) DFG-out, Asp-381 protonated. At thermodynamic equilibrium at temperature T, the relative population of the DFG-out conformation decreases with increasing pH as (see *SI Text*)

$$P_{\text{out}} = \frac{1}{1 + \exp(\Delta G_{2\to 3}/RT) + \exp(\Delta G_{2\to 3}/RT + [\text{pH} - \text{p}K_{\text{a,in}}] \times \log_e 10)}, \quad [1]$$

where $\Delta G_{2\to 3}$ is the free-energy cost of the DFG flip from DFG-in to DFG-out with Asp-381 protonated, R is the gas constant, and $\text{p}K_{\text{a,in}}$ is the $\text{p}K_{\text{a}}$ of Asp-381 in a DFG-in conformation (i.e., it is the hypothetical $\text{p}K_{\text{a}}$ when DFG-out states are excluded, and thus differs from the actual $\text{p}K_{\text{a}}$).

At equilibrium, one might anticipate DFG-in conformations to dominate, because the aspartate and phenylalanine residues are favorably placed in environments matching their polarity. Three other factors combined, however, may tip the thermodynamic balance in favor of DFG-out conformations. First, in the DFG-out conformation of Abl, which we model on the kinase domain of c-Abl PDB ID code 1OPK (7), Asp-381 is well positioned to form a hydrogen bond with the exposed backbone carbonyl of Val-299. Second, contrary to what one might expect given the preponderance of reported kinase structures that appear in the DFG-in conformation, we find that the ϕ–ψ angles of the DFG aspartate in active Abl, and in most other DFG-in kinase structures, fall within the unusual left-handed helix region of Ramachandran space (Fig. S4*B*), indicating a more strained main-chain configuration for DFG-in than DFG-out. Third, standard electrostatics calculations (30) suggest that Asp-381 has an elevated value of $\text{p}K_{\text{a,in}}$ in the absence of the ATP-bound magnesium ion, due in part to the influence of the conserved residues Glu-286, Asp-363, and Asn-368. Analysis of kinase crystal structures as a function of crystallization buffer pH (Fig. S4*C*) also suggests that an elevated $\text{p}K_{\text{a,in}}$ may occur in other kinases.

Combining standard literature estimates (35) and simulation results (see *SI Text*), we have estimated the contributions to $\Delta G_{2\to 3}$ and we find $\Delta G_{2\to 3} \approx -1.1$ kcal/mol. The electrostatics calculations yield $\text{p}K_{\text{a,in}} \approx 6.6$. With these estimates, Eq. **1** gives a large relative population of DFG-out conformations at pH ≈6 that decreases rapidly around pH ≈7 (Fig. 4*B*). Although the estimated parameters are, of course, only semiquantitative, the basic conclusion of a near-balance in the free energies of DFG-in and DFG-out conformations close to physiological pH is robust to moderate changes in the parameters. Importantly, Eq. **1** shows that with a small $\Delta G_{2\to 3}$, the DFG conformation becomes sensitive to changes in $\text{p}K_{\text{a,in}}$ and can thus be controlled by electrostatic changes in the ATP-binding site (we discuss the potential significance of this observation to kinase catalysis below). Similarly, our model predicts the effect of mutating Asp-381 or Phe-382 on DFG conformation; replacing Phe-382 with a less hydrophobic residue, for example, increases the relative population of DFG-out (Fig. 4*B*).

Our energetic model should also be applicable to other kinases, most directly if their activation loops adopt the common open conformation (22, 36) in DFG-in and DFG-out states (as do Abl and c-Abl in PDB ID codes 2F4J (22) and 1OPK (7), respectively). Other activation-loop conformations—particularly those occluding substrate binding, as in Abl–imatinib complexes such as PDB ID code 1IEP (8)—can lead to solvent exposure of both Asp-381 and Phe-382. Such structures are found to adopt DFG-out conformations. This observation is consistent with our analysis, because the key factor stabilizing DFG-in conformations (the hydrophobic packing of Phe-382) is missing from these structures.

Probing the DFG-out Conformation by Using Abl–Imatinib Binding. With imatinib bound, Abl adopts a DFG-out conformation (8), suggesting that imatinib binding kinetics may provide a probe of DFG conformation. We derived the on-rate constant, k_{on}, of imatinib binding to Abl as a function of pH by using stopped-flow fluorescence assays. As shown in Fig. 4*A*, k_{on} for wild-type Abl decreases by nearly an order of magnitude as pH increases from 5.5 to 7.5, in which range imatinib is predominantly neutral (37). We

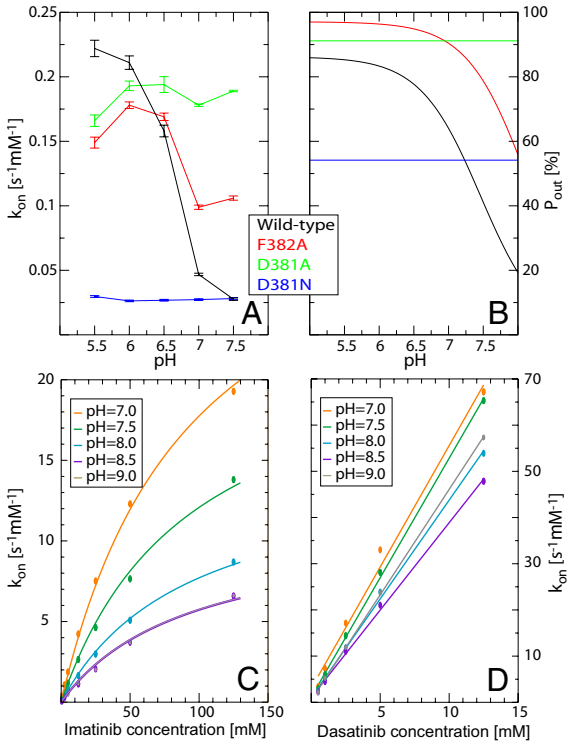

Fig. 4. pH dependence of Abl-imatinib binding. (*A*) The on-rate constant of imatinib binding to wild-type Abl and to 3 mutants as a function of pH, as measured by stopped-flow tryptophan fluorescence assays. The error bars indicate the uncertainty of the linear regression fit to the observed rates from which the on-rate constants are obtained. (*B*) The relative population of DFG-out estimated according to Eq. **1**. The similarity between the model results for P_{out} and the experimental k_{on} values supports our interpretation of the experimental data and the factors underlying DFG flips. (*C*) The observed fluorescence-decay rates for Abl-imatinib binding rates at 5 different pH values (virtually identical at pH 8.5 and pH 9). The solid lines are obtained from independent 2-parameter fits using the proposed kinetic scheme (see *SI Text* for details). (*D*) The dasatinib binding rate constants for wild-type Abl measured at 5 different pH values show only weak pH dependence. The lines are linear fits to the data.

observed a very similar pH dependence for a c-Abl construct containing its kinase and SH2-SH3 domains (Fig. S2*A*). However, control experiments showed the imatinib-binding kinetics for Abl mutants D381A and D381N to have essentially no dependence on pH over the same range (Fig. 4*A*). The results for the mutants strongly suggest that the pH dependence observed for the wild type was a result of protonation at Asp-381.

Independent structural evidence supporting protonation of Asp-381 also exists. Most convincingly, the DFG-out c-Abl structure (PDB ID code 1OPK, resolution 1.8 Å, crystallized at pH 7.0) (7) shows 1 Asp-381 side-chain oxygen to be only 2.8 Å away from the Val-299 backbone carbonyl oxygen in a position that would be hard to rationalize if Asp-381 were not protonated in this structure. In addition, our analysis of the representative kinase structures (restricted to DFG-in conformations without bound ligands) shows that the distance of the DFG aspartate from the conserved lysine (Lys-271 in Abl) generally increases with decreasing pH of the crystallization buffer (Fig. S4*C*). This suggests that protonation of the DFG aspartate may be common in protein kinases.

The above results provide strong evidence that the $\text{p}K_{\text{a}}$ of Asp-381 is significantly raised above typical values for aspartate residues. Because imatinib is a DFG-out binder (8), another natural conclusion from the data is that protonation of Asp-381 favors DFG-out conformations. As a negative control, we have also performed fluorescence experiments using the DFG-in binder

dasatinib (38, 39). It is thought that so-called DFG-in binders typically bind to both DFG-in and DFG-out conformations (13). We find only a very weak pH dependence for dasatinib binding (Fig. 4*D*), consistent with the interpretation that the pH dependence observed for imatinib binding is a result of a pH-dependent DFG conformation.

More evidence supporting a link between protonation and DFG conformation comes from the pH dependence of imatinib binding to the Abl mutant F382A shown in Fig. 4*A*. This mutant shows a decrease in the imatinib on-rate constant with increasing pH, although the decrease is less pronounced and shifted to higher pH compared with the wild type. This implies a higher pK_a for Asp-381 in the mutant, despite the fact that both phenylalanine and alanine are nonpolar and are positioned away from Asp-381, indicating that the mutation causes a conformational change and hence the elevated pK_a. As explained above, an F382A mutation is predicted to lead to a larger population of DFG-out conformations, thus raising the pK_a of Asp-381 in agreement with our experimental observations.

Kinetic Scheme for Imatinib Binding. In contrast to its kinetics, the thermodynamics of Abl–imatinib binding determined from isothermal titration calorimetry (ITC) do not show a clear pH dependence (see Table S2). This is consistent with the observation made above that in the Abl–imatinib complex—unlike in the apo DFG-out conformation—Asp-381 is solvent-exposed (because of rearrangement of the activation loop on binding; see Fig. S5*A*). To provide a quantitative explanation for the pH-dependent imatinib-binding kinetics, we propose the following kinetic scheme:

$$\begin{array}{ccc} \mathrm{Abl^-(DFG\text{-}in)} & \underset{k_{-0}}{\overset{k_{+0}}{\rightleftharpoons}} & \mathrm{Abl^H(DFG\text{-}in)} \\ & & k_{+1} \updownarrow k_{-1} \\ \mathrm{Abl(DFG\text{-}out)} + \mathrm{imatinib} & \underset{k_{-2}}{\overset{k_{+2}}{\rightleftharpoons}} & \mathrm{Abl\text{-}imatinib}, \end{array} \quad [2]$$

where $\mathrm{Abl^H}$ and $\mathrm{Abl^-}$ denote Abl with and without protonation of Asp-381. For the imatinib concentrations ($<12.5\ \mu$M) used in our experiments (discussed above), the fluorescence relaxation data fits a single-exponential decay, and the resultant relaxation rates are found to increase linearly with imatinib concentration (Fig. S6). Under these conditions, we thus assume that the Asp-381-protonation and DFG-flip steps of the kinetic scheme (the leftmost and middle steps in Eq. **2**, respectively) are fast compared with imatinib binding to the DFG-out conformation (rightmost step in Eq. **2**). This leads to effective 1-step kinetics with an on-rate constant proportional to the population of the DFG-out state: $k_{on} = P_{out}k_{+2}$. In Fig. 4*B*, we show our estimates for P_{out} (Eq. **1**) as a function of pH for Abl and 3 mutants. These estimates are clearly consistent with our experimental results for k_{on}, supporting our interpretation that the protonation of Asp-381 increases the population of DFG-out.

At sufficiently high imatinib concentrations, the rate of imatinib binding to the DFG-out conformation should become comparable with that of the DFG flip. In this case, the kinetic scheme leads to effective 2-step kinetics. This is consistent with the observed fluorescence decay rates, k_{obs}, which are found to deviate from a linear dependence on imatinib concentration (see Fig. 4*C*). In contrast, similar experiments for dasatinib binding showed no clear deviation from linearity (Fig. 4*D*). These results clearly demonstrate an intermediate step in imatinib binding, and support the interpretation that the pH dependence of imatinib binding arises from the DFG flip. Detailed analysis of the kinetic data of imatinib binding also revealed the DFG-flip time scale to be in the tens of milliseconds (see *SI Text*), which is consistent with NMR studies of DFG dynamics (13). This relatively long time scale may reflect the fact that the DFG flip involves conformational changes of the activation loop beyond the DFG motif itself (33).

Conservation of the DFG Motif and Its Role in Kinase Catalysis. Although the DFG aspartate is clearly important for catalysis, the roles of the phenylalanine and glycine residues and the reason for their conservation are much less certain (40). Our results provide evidence that both of these residues may be essential to DFG conformational change. We find that the phenylalanine plays a key role in maintaining an energetic balance between the DFG-in and DFG-out states by compensating for the unfavorable DFG aspartate backbone torsion angles adopted in the DFG-in conformation. Our simulations also show that the DFG flip involves extensive backbone-torsion motions at the glycine residue, suggesting that the unique flexibility of glycine may serve to lower the kinetic barrier for the flip. This is consistent with work (41) suggesting that the DFG motif is optimized for functional dynamics rather than for structural stability, as is our finding that the DFG-out conformation can be populated under physiological conditions even in the absence of DFG-out binders.

If the DFG flip is to explain the conservation of the DFG motif, its role in kinase function must extend beyond the specific activation mechanism of c-Abl. The DFG flip has been suggested to promote ADP release (27), the rate-limiting step in kinase catalysis (42–44). Intriguingly, our results could be interpreted as hinting at a mechanistic explanation for such a proposed role. In ATP-bound kinases, the DFG aspartate interacts with a catalytically essential magnesium ion (Mg^{2+}) 2.3 Å away, which in turn coordinates the β and γ phosphates of ATP (5). Encouraged by observations on small G proteins (45, 46) showing that Mg^{2+} binding is weakened by $\approx$3 orders of magnitude after transfer of the γ phosphate, we speculate that in kinases, this Mg^{2+} may likewise be released after phosphate transfer, thus reducing the positive charge in the immediate vicinity of the DFG aspartate. If this is the case, we predict that this change in the electrostatic environment of the DFG aspartate would lead to its protonation—either from the solvent or through proton transfer from the catalytic base Asp-363—causing the motif to flip to a DFG-out conformation and thus facilitating ADP release. In such a scenario, nucleotide release could, in principle, be regulated by magnesium, consistent with the experimental observation that the ADP-release rate decreases with increasing Mg^{2+} concentration (44).

The DFG flip could facilitate ADP release, and potentially binding of the ATP-Mg^{2+} complex, by allowing the kinase to adopt a DFG-out conformation, which we find to be significantly more flexible in terms of interlobe motions than the DFG-in conformation (Fig. S7). This increased flexibility is consistent with the finding (32) that, in the active conformation, the DFG phenylalanine is part of the "hydrophobic spine" that lends stability to the DFG-in conformation. Although speculative, our suggestions are also consistent with kinetic data showing that at physiological Mg^{2+} concentration, a 10-ms time scale conformational change follows ATP binding and precedes ADP release (44), as well as with recent NMR titration experiments showing that upon the binding of ATP to PKA kinase, the DFG motif and nucleotide-binding loop of PKA exhibit microsecond to millisecond dynamics (31).

Conclusion

Using Abl as a model system, we have simulated the DFG flip, a conformational change known to be significant in a diverse set of kinases and, in particular, to be an important switch for c-Abl activation (7). The simulations highlight the role of large-scale conformational changes in facilitating the DFG flip and point to the importance of the protonation of the DFG aspartate residue. This conclusion is supported experimentally by our Abl-imatinib binding assays, which reveal markedly pH-dependent binding

kinetics. Our analysis shows that the DFG conformation is determined by a number of opposing factors that approximately balance, resulting in a DFG conformation sensitive to small changes in the electrostatics of the ATP-binding site. Combined with existing structural and kinetic data, this leads us to suggest that the conservation of the DFG motif stems from the DFG flip, which switches the kinase from the less-flexible DFG-in form required for catalysis to the more-flexible DFG-out form that facilitates nucleotide binding and release. The set of intermediate conformations observed in our simulations of the DFG flip may present new opportunities for inhibitor design. Furthermore, the pH sensitivity of the DFG conformation raises the possibility that local pH variations may play a role in kinase regulation in vivo.

Materials and Methods

Additional details are provided in *SI Text*.

Simulation Details. All simulations used the simple point charge (SPC) model for water (47), the standard OPLS-AA parameters for ions (48, 49), and the OPLS-AA/L force field for proteins (28, 29) as provided by the program IMPACT (50) (note that the relevant force-field option, referred to as OPLS_2003 in the IMPACT paper, has subsequently been renamed as OPLS_2005 in the actual program). All molecular dynamics simulations were performed by using the parallel MD program Desmond (19) on 64 or 128 dual-processor Opteron nodes connected by a high-speed Infiniband network (Topspin, San Jose, CA). Each simulation is represented by a code number that is given, along with other key simulation details, in Table S1.

Kinetic Measurements of Drug Binding. Wild-type human c-Abl kinase domain (residues 248–532) and mutant proteins were generated and purified as described previously (51). The drug-binding kinetics is measured by monitoring the decrease of protein fluorescence at 350 nm upon excitation at 290 nm on a HORIBA Jobin Yvon FluoroMax-3 spectrofluorimeter for 10–20 half-lives of the transient, recorded by 1,000–2,000 data points.

ACKNOWLEDGMENTS. We thank I. Arkin, D. Borhani, B. Gregersen, M. Jacobson, J. Klepeis, K. Lindorff-Larsen, P. Maragakis, and A. Wang for helpful discussions and critical reading of the manuscript. We also thank S. Miller for use of the stopped-flow equipment. M.A.S. is supported by National Institutes of Health Grant 5K99GM080097.

1. Manning G, Whyte DB, Martinez R, Hunter T, Sudarsanam S (2002) The protein kinase complement of the human genome. *Science* 298:1912–1934.
2. Futreal PA, *et al.* (2004) A census of human cancer genes. *Nature Rev Cancer* 4:177–183.
3. Cohen P (2002) Protein kinases—The major drug targets of the twenty-first century? *Nat Rev Drug Discov* 1:309–315.
4. Greenman C, *et al.* (2007) Patterns of somatic mutation in human cancer genomes. *Nature* 446:153–158.
5. Zheng JH, *et al.* (1993) Crystal structure of the catalytic subunit of cAMP-dependent protein-kinase complexed with MgATP and peptide inhibitor. *Biochem* 32:2154–2161.
6. Bossemeyer D, *et al.* (1993) Phosphotransferase and substrate binding mechanism of the cAMP-dependent protein kinase catalytic subunit from porcine heart as deduced from the 2.0 A structure of the complex with Mn2+ adenylyl imidodiphosphate and inhibitor peptide PKI(5–24). *EMBO J* 12:849–859.
7. Nagar B, *et al.* (2003) Structural basis for the autoinhibition of c-Abl tyrosine kinase. *Cell* 112:859–871.
8. Schindler T, *et al.* (2000) Structural mechanism for STI-571 inhibition of abelson tyrosine kinase. *Science* 289:1938–1942.
9. Demetri GD, *et al.* (2002) Efficacy and safety of imatinib mesylate in advanced gastrointestinal stromal tumors. *N Engl J Med* 347:472–480.
10. Kantarjian H, *et al.* (2002) Hematologic and cytogenetic responses to imatinib mesylate in chronic myelogenous leukemia. *N Engl J Med* 346:645–652.
11. Noble MEM, Endicott JA, Johnson LN (2004) Protein kinase inhibitors: Insights into drug design from structure. *Science* 303:1800–1805.
12. Liu Y, Gray NS (2006) Rational design of inhibitors that bind to inactive kinase conformations. *Nat Chem Biol* 2:358–364.
13. Vogtherr M, *et al.* (2006) NMR characterization of kinase p38 dynamics in free and ligand-bound forms. *Angew Chem Int Ed* 45:993–997.
14. Gullingsrud J, Kim C, Taylor SS, McCammon JA (2006) Dynamic binding of PKA regulatory subunit RI alpha. *Structure (London)* 14:141–149.
15. Young MA, Gonfloni S, Superti-Furga G, Roux B, Kuriyan J (2001) Dynamic coupling between the SH2 and SH3 domains of c-Src and hck underlies their inactivation by C-terminal tyrosine phosphorylation. *Cell* 105:115–126.
16. Faraldo-Gómez JD, Roux B (2007) On the importance of a funneled energy landscape for the assembly and regulation of multidomain Src tyrosine kinases. *Proc Natl Acad Sci USA* 104:13643–13648.
17. Levinson NM, *et al.* (2006) A Src-like inactive conformation in the Abl tyrosine kinase domain. *PLoS Biol* 4:753–767.
18. Shaw DE (2005) A fast, scalable method for the parallel evaluation of distance-limited pairwise particle interactions. *J Comput Chem* 26:1318–1328.
19. Bowers KJ, *et al.* (2006) Scalable algorithms for molecular dynamics simulations on commodity clusters. *Proceedings of the ACM/IEEE Conference on Supercomputing (SC06)* (ACM Press, New York).
20. Bowers KJ, Dror RO, Shaw DE (2006) The midpoint method for parallelization of particle simulations. *J Chem Phys* 124:184109–184111.
21. Bowers KJ, Dror RO, Shaw DE (2007) Zonal methods for the parallel execution of range-limited N-body simulations. *J Comput Phys* 221:303–329.
22. Young MA, *et al.* (2006) Structure of the kinase domain of an imatinib-resistant Abl mutant in complex with the aurora kinase inhibitor VX-680. *Cancer Res* 66:1007–1014.
23. De Bondt HL, *et al.* (1993) Crystal structure of cyclin-dependent kinase 2. *Nature* 363:595–602.
24. Xu W, Harrison SC, Eck MJ (1997) Three-dimensional structure of the tyrosine kinase c-Src. *Nature* 385:582–585.
25. Sicheri F, Moarefi I, Kuriyan J (1997) Crystal structure of the Src family tyrosine kinase Hck. *Nature* 385:602–609.
26. Wood ER, *et al.* (2004) A unique structure for epidermal growth factor receptor bound to GW572016 (lapatinib): Relationships among protein conformation, inhibitor off-rate, and receptor activity in tumor cells. *Cancer Res* 64:6652–6659.
27. Kannan N, Neuwald AF (2005) Did protein kinase regulatory mechanisms evolve through elaboration of a simple structural component? *J Mol Biol* 351:956–972.
28. Jacobson MP, Kaminski GA, Friesner RA, Rass SC (2002) Force field validation using protein side chain prediction. *J Phys Chem B* 106:11673–11680.
29. Kaminski GA, Friesner RA, Tirado-Rives J, Jorgensen WL (2001) Evaluation and reparametrization of the OPLS-AA force field for proteins via comparison with accurate quantum chemical calculations on peptides. *J Phys Chem B* 105:6474–6487.
30. Gordon JC, *et al.* (2005) H++: A server for estimating pK(a)s and adding missing hydrogens to macromolecules. *Nucleic Acids Res* 33:W368–371.
31. Masterson LR, Mascioni A, Traaseth NJ, Taylor SS, Veglia G (2008) Allosteric cooperativity in protein kinase A. *Proc Natl Acad Sci USA* 105:506–511.
32. Kornev AP, Haste NM, Taylor SS, Ten-Eyck LF (2006) Surface comparison of active and inactive protein kinases identifies a conserved activation mechanism. *Proc Natl Acad Sci USA* 103:17783–17788.
33. Nolen B, Taylor SS, Ghosh G (2004) Regulation of protein kinases: Controlling activity through activation segment conformation. *Mol Cell* 15:661–675.
34. Honig BH, Hubbell WL (1984) Stability of salt bridges in membrane-proteins. *Proc Natl Acad Sci USA* 81:5412–5416.
35. Kyte J, Doolittle RF (1982) A simple method for displaying the hydropathic character of a protein. *J Mol Biol* 157:105–132.
36. Huse M, Kuriyan J (2002) The conformational plasticity of protein kinases. *Cell* 109:275–282.
37. Szakacs Z, *et al.* (2005) Acid-base profiling of imatinib (gleevec) and its fragments. *J Med Chem* 48:249–255.
38. Tokarski JS, *et al.* (2006) The structure of dasatinib (BMS-354825) bound to activated ABL kinase domain elucidates its inhibitory activity against imatinib-resistant ABL mutants. *Cancer Res* 66:5790–5797.
39. Shah NP, *et al.* (2004) Overriding imatinib resistance with a novel ABL kinase inhibitor. *Science* 305:399–401.
40. Adams JA (2001) Kinetic and catalytic mechanisms of protein kinases. *Chem Rev* 101:2271–2290.
41. Bukhtiyarova M, Karpusas M, Northrop K, Namboodiri HVM, Springman EB (2007) Mutagenesis of p38 alpha MAP kinase establishes key roles of Phe169 in function and structural dynamics and reveals a novel DFG-out state. *Biochemistry* 46:5687–5696.
42. Lew J, Taylor SS, Adams JA (1997) Identification of a partially rate-determining step in the catalytic mechanism of cAMP-dependent protein kinase: A transient kinetic study using stopped-flow fluorescence spectroscopy. *Biochemistry* 36:6717–6724.
43. Shaffer J, Sun GQ, Adams JA (2001) Nucleotide release and associated conformational changes regulate function in the COOH-terminal Src kinase, Csk. *Biochemistry* 40:11149–11155.
44. Shaffer J, Adams JA (1999) Detection of conformational changes along the kinetic pathway of protein kinase A using a catalytic trapping technique. *Biochemistry* 38:12072–12079.
45. Simon I, Zerial M, Goody RS (1996) Kinetics of interaction of Rab5 and Rab7 with nucleotides and magnesium ions. *J Biol Chem* 271:20470–20478.
46. Shutes A, Phillips RA, Corrie JE, Webb MR (2002) Role of magnesium in nucleotide exchange on the small G protein rac investigated using novel fluorescent guanine nucleotide analogues. *Biochem* 41:3828–3835.
47. Berendsen HJC, Postma JPM, van Gunsteren WF, Hermans J (1981) in *Intermolecular Forces*, ed Pullman B (D. Reidel, Dordrecht, The Netherlands), pp 331–342.
48. Åqvist J (1990) Ion–water interaction potentials derived from free energy perturbation simulations. *J Phys Chem* 94:8021–8024.
49. Jorgensen WL, Ulmschneider JP, Tirado-Rives J (2004) Free energies of hydration from a generalized born model and an all-atom force field. *J Phys Chem B* 108:16264–16270.
50. Banks JL, *et al.* (2005) Integrated modeling program, applied chemical theory (IMPACT). *J Comput Chem* 26:1752.
51. Seeliger MA, *et al.* (2005) High yield bacterial expression of active c-Abl and c-Src tyrosine kinases. *Protein Sci* 14:3135–3139.